A study on dynamic desorption process of methane in slits

Lei Chen [*], Ding-Bin Huang, Shan-You Wang, Yi-Nan Nie, Ya-Ling He, Wen-Quan Tao

Key Laboratory of Thermo-Fluid Science and Engineering, Ministry of Education, School of Energy & Power Engineering, Xi'an Jiaotong University, Xi'an, Shaanxi, 710049, People's Republic of China

ABSTRACT

The desorption behavior of methane in slit was studied in this paper. We build a differential equation which describe dynamic desorption process, and propose a correction method. The mass transfer resistance in free region is considered and the accuracy of the result is improved using this correction method. Based on differential equation, the effects of pressure, temperature and solid material on dynamic desorption speed are analyzed. Desorption becomes faster when pressure increases. When pressure is low, desorption speed increases with increasing temperature; oppositely, desorption speed decreases with increasing temperature. When pressure is low, the desorption speed at different wall material is quartz > kaolinite > graphite; when pressure is high, the desorption speed is quartz > graphite > kaolinite.

© 2019 Elsevier Ltd. All rights reserved.

1. Introduction

China is rich in shale gas resources. The United States Energy Information Administration estimates the recoverable shale gas resources in China to be thirty-six trillion cubic metres, which accounts for 20% of the total shale gas recoverable resources, ranking China as first in the world [1]. Exploitation of shale gas is important for Chinese energy security. Adsorption, desorption and flow of shale gas are important processes in shale gas exploration [2—12]. The main component of shale gas is methane. There are different definitions of desorption from different angles. From the viewpoint of a single adsorbent particle, desorption is a phenomenon in which the adsorbent particles are released from the surface of the adsorbent, i.e., the process by which the adsorbate particles are converted from the adsorbed state to free state [2,3] ("micro-desorption" is used below to refer to this process). When the adsorbate/adsorbent system is in equilibrium, the micro-adsorption process (the adsorbate particles are converted from the free state to the adsorbed state) and the micro-desorption process are present at the same rate. From the point of view of the total adsorbate, desorption is a process in which the total amount of adsorbed adsorbate is reduced ("macro-desorption" is used below to refer to this process). Macroscopic desorption occurs, the system is in a non-equilibrium state, the rate of micro-

desorption is greater than the rate of microscopic adsorption. The phenomenon of macroscopic desorption can be caused by pressure reduction, temperature and other factors. Microscopic desorption can exist in equilibrium and non-equilibrium states, macroscopic desorption only exists in the non-equilibrium process. The desorption referred to in engineering applications is usually macroscopic desorption [4,13—24].

During shale gas extraction, shale gas is continuously withdrawn from gas wells [25—32], resulting in the decrease in pressure in the reservoir, which triggers a macroscopic desorption process of shale gas in the reservoir [5—7,33—35]. Shale gas desorption plays an important role in the production of shale gas reservoirs and typically increases by 5%—15% at the end of production [8]. The study of shale gas desorption behavior will help to better understand the transport process of shale gas in gas reservoirs, thus more accurately predict yield and productivity [9,10,34—36].

In this paper, the microscopic adsorption and desorption processes in the slit in the equilibrium state are studied. The differential equations derived from the Langmuir model can well describe the macroscopic desorption process. However, when the mass transfer resistance inside the slit is large, it will have a significant effect on macroscopic desorption. We will present an improved measure to consider the mass transfer resistance inside the slit, which can make the solution of the differential equation more consistent with the actual situation. Besides, the effect of pressure, temperature and wall material on desorption process was also studied.

* Corresponding author.
E-mail address: chenlei@mail.xjtu.edu.cn (L. Chen).

2. Microscopic adsorption and microscopic desorption in equilibrium state

The Langmuir model [11,37–42] is a classical model that describes physical adsorption and has the advantage of simple structure. According to the Langmuir adsorption model, the micro-adsorption and micro-desorption rates can be expressed as:

$$J_a = k_a(1 - \theta)P/P_0 \tag{1}$$

$$J_d = k_d\theta \tag{2}$$

where :

J_a, J_d —— The rate of microscopic adsorption and microscopic desorption, mol/(m^2 s);
k_a, k_d —— The rate constant of microscopic adsorption and microscopic desorption, mol/(m^2 s);
θ—— Adsorbent surface coverage;
P, P_0 —— Pressure and reference pressure, MPa;

When microscopic adsorption progress and microscopic desorption progress are in equilibrium:

$$J_a = J_d \tag{3}$$

We can obtain Langmuir isothermal adsorption curve by Eqs. (1)–(3):

$$\theta = \frac{c_s}{c_{sat}} = \frac{1}{\frac{k_d P_0}{k_a P} + 1} \tag{4}$$

where :

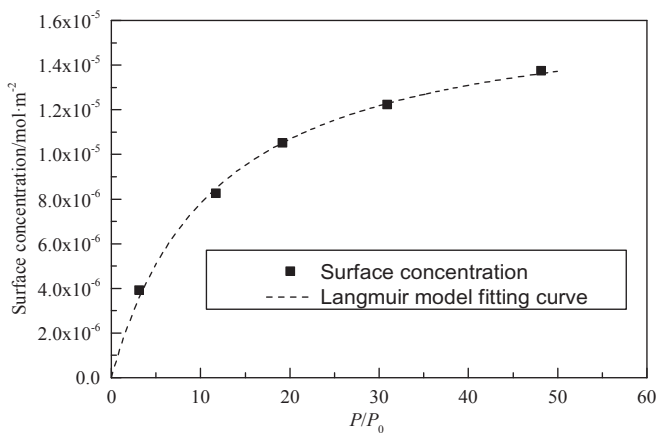c_s —— Adsorbent surface adsorbate concentration, mol/m^2 ;

Fig. 1. The Langmuir isothermal adsorption curve which was fitted with simulated results of methane adsorption in a 3.6 nm graphite slab at 353.5 K.

c_{sat} —— Adsorbent surface adsorbate saturation concentration, mol/m^2

To obtain the relationship between c_s and P/P_0, set the reference pressure P_0 1 MPa. In the calculation of the surface concentration of adsorbate, we select the first and second layer of adsorption layer as the adsorption area, the amount of adsorbed methane corresponding to the unit area of solid wall is the surface concentration. In order to obtain c_{sat}, the relationship between c_s and P/P_0 needs to be fitted by using Eqn. (4). The fitting results are shown in Fig. 1. It can be seen from the figure that the Langmuir isothermal adsorption equation can describe the adsorption behavior of methane on graphite surface. The saturation density c_{sat} of the adsorption of methane on the graphite surface at 353.5 K is 1.69×10^{-5} mol/m^2, and the ratio k_a/k_d of the microscopic desorption rate constant to the microscopic adsorption rate constant is 11.66.

In order to obtain the rate constants of microscopic adsorption and microscopic desorption, microscopic adsorption and microscopic desorption rates should also be monitored. The adsorption behavior of methane in the graphite slit was simulated by molecular dynamics simulation. We first carried out simulations of methane adsorption in a 3.6 nm graphite slit in which there are 438 methane molecules at 353.5 K, the periodic boundary condition is conducted, the NVT system was adopted with a time step of 3 fs, the pressure in the slit was about 30.5 MPa, Nose-Hoover maintains a temperature of 353.5 K and a relaxation time of 300 fs. The first 1.05 ns after the start of the simulation is used to balance the system and the density distribution is counted from 1.05 to 1.5 ns. Then, and the microscopic adsorption and microscopic desorption flux of 0.45 ns were calculated after the equilibrium was carried out under 353.5 K temperature. The division method of fitting Langmuir isotherms from above is used in the adsorption zone. Since the statistical system is in equilibrium, the microscopic adsorption rate is equal to the microscopic desorption rate.

Table 1 summarizes the adsorption of methane in a 3.6 nm graphite slit at 353.5 K. Using Eq. (2), the microscopic desorption rate constant k_d can be obtained by fitting the microscopic desorption rate J_d and the surface coverage θ. As shown in Fig. 2, the microscopic desorption rate is approximately proportional to the surface coverage, although sometimes the pressure is slightly higher and lower, but the deviation is within acceptable limits. We can get that the value of the microscopic desorption rate constant k_d is 4.96×106 mol/(m^2·s) from Fig. 2 , and then we can get the value of k_a is 4.25×105 mol/(m^2 s) by the k_a/k_d value obtained by the Langmuir isotherm fitting.

The above studies show that the Langmuir adsorption model can not only describe the relationship between the amount of methane in the adsorbed state and the pressure, but also the relationship between the rate of microscopic adsorption and desorption and the pressure and the surface coverage. In the next section, we will establish the differential equation describing macroscopic desorption progress in the non-equilibrium state. Comparing the differential equation solution and the molecular dynamics simulation results, it shows that these conclusions are still suitable in the non-equilibrium state.

Table 1
Estimation of methane adsorption simulation under 353 K condition.

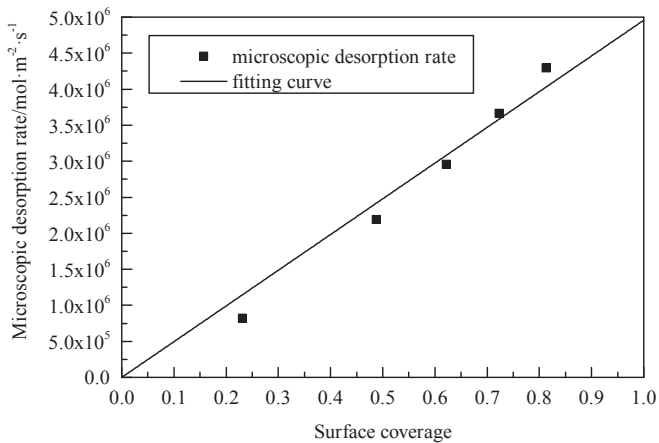| Group	1	2	3	4	5
Number of methane molecules	100	250	340	438	530
Pressure (MPa)	3.14	11.72	19.19	30.95	48.18
Surface concentration c_s (mol/m^2)	3.91×10^{-6}	8.24×10^{-6}	1.05×10^{-5}	1.22×10^{-5}	1.37×10^{-5}
Surface coverage ratio/θ	0.23	0.49	0.62	0.72	0.81
Microscopic adsorption (desorption) rate/J_a (J_d) [mol/(m^2 s)]	8.21×10^5	2.19×10^6	2.96×10^6	3.66×10^6	4.29×10^6

Fig. 2. The relationship between microscopic desorption rate and surface coverage.

3. Macroscopic desorption process in the non-equilibrium state

3.1. Differential equation on the macroscopic desorption process

The concentration of methane in the slit is only related to pressure but not to time. It can be considered as equilibrium state. But the exploitation of shale gas is inevitably a diffusion process from micro-pore to fracture, so it is inevitably a non-equilibrium state, that is to say, when the macroscopic desorption occurs, the microscopic desorption rate is greater than the microscopic adsorption rate, resulting in a decrease in the total amount of adsorbed adsorbate. In the practical engineering application, the macroscopic desorption process is more concerned than the microscopic desorption process. We can know how much adsorbent can be released in a macroscopic desorption process through the study of equilibrium. We can obtain the relationship between the amount of released adsorbent and time by the study of non-equilibrium macroscopic desorption process. Furtherly, we can establish the differential equation describing the methane coverage of the graphite surface:

$$\frac{d\theta}{dt} = \frac{J_a - J_b}{c_{sat}} = \frac{k_a(1-\theta)P(t)/P_0 - k_d\theta}{c_{sat}} \tag{5}$$

If the pressure condition $P(t)$ at each moment in the slit is known, the change of the methane coverage of the graphite surface with time can be obtained by using Eqn. (5), and the amount of adsorbed methane at each time can be calculated. When $P(t)$ is relatively simple, the above equation can be directly obtained analytical solution. For example, the solution of the equation is obtained when P is a constant as follows:

$$\frac{\theta(t) - \theta(0)}{\theta(+\infty) - \theta(0)} = 1 - \exp\left[-\frac{(k_aP + k_d)}{c_{sat}}t\right] \tag{6}$$

where:

$$\theta(+\infty) = \frac{1}{\frac{k_dP_0}{k_aP} + 1} \tag{7}$$

It can be seen from Eq. (6) that $c_{sat}/(k_aP + k_d)$ has a time dimension and can be regarded as the time constant of the macroscopic desorption process. It is the decisive factor that affects the speed of the macroscopic desorption process. The value of $c_{sat}/(k_aP + k_d)$ is larger, the macroscopic desorption process goes faster.

When P changes with time, $c_{sat}/(k_aP + k_d)$ can still be used to qualitatively judge the speed of macro-desorption process.

3.2. Molecular dynamics simulation of macroscopic desorption process

In order to verify the correctness of Eq. (5), we use molecular dynamics simulation (MDS) to simulate a macroscopic desorption process [12,13,23–27] and compare this process with the results of Eq. (5). Here 438 methane molecules were filled in the slit, NVT is adopted, the Nose-Hoover temperature control method was used to maintain the temperature of 353.3 K, the time step was 1 fs, the equilibrium state was reached after 1 ns, the equilibrium pressure was 30.95 MPa and the other model parameters were the same as those used in the previous simulation. Remain the coordinates and velocity of methane molecules in the adsorption zone unchanged, and then remove all methane molecules in the free zone to simulate a sudden pressure drop. The remaining 245 methane molecules in the slit continue the NVT simulation 15 ps, and stat the number of methane molecule in the adsorption zone during each time step. Fig. 3 shows the methane molecules distribution, and the number of methane molecule in the adsorption zone decreases with time shown in Fig. 4.

3.3. Solving macroscopic desorption process by differential equation

The following process is used to predict the process by Eq. (5). $P(t)$ must be known to work out the solution. However, in the simulation of molecular dynamics, we only know that the initial pressure is zero. The subsequent pressure changes are related to the degree of macro-desorption: the more adsorbed methane is released during macro-desorption, the greater the pressure in the slit. In order to solve Eq. (5), A relationship between the number of methane molecules in the free zone and pressure should be added.
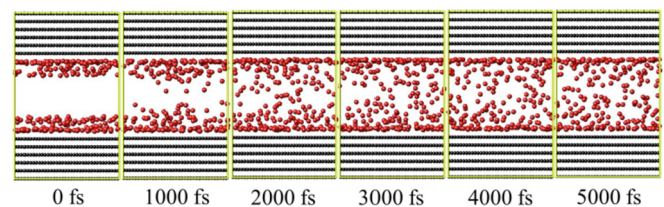

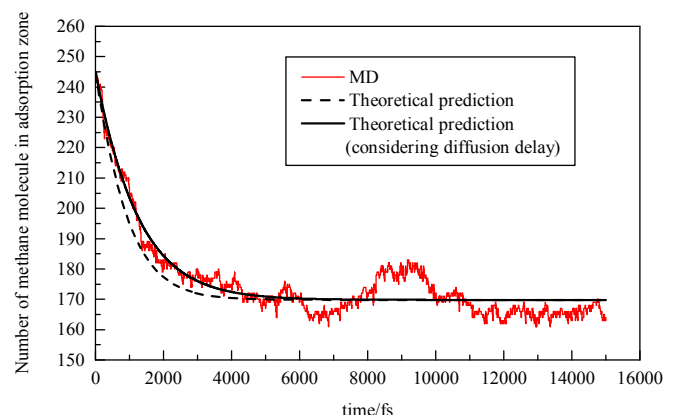**Fig. 3.** Molecular Dynamics Simulation of Macroscopic desorption.

Fig. 4. The change of methane number in the adsorption zone with time.

Assuming that the methane molecules in the free zone are evenly distributed, the methane density in the free zone can be calculated according to the number of methane molecules in the free zone, and the free zone pressure can be obtained by the $P(\rho, T)$. So the pressure can be obtained:

$$P = 0.1547N_f + 0.0907 \tag{8}$$

where:

N_f ——Number of methane molecules in free zone
P —— Pressure in the slit, MPa

Substitute Eq. (8) into Eq. (5), then we get:

$$\frac{dN_a}{dt} = \frac{k_a(SN_Ac_{sat} - N_a)[0.1547(245 - N_a) + 0.0907]/P_0 - k_dN_a}{c_{sat}}$$
$$= f(N_a) \tag{9}$$

where :

N_a——Number of methane molecules in adsorption area;
S —— The graphite surface area in the simulated box (the sum of the area of the upper and lower walls);
N_A —— Avogadro constant, 6.02×10^{23};

Solve Eq. (9) by numerical method. Eqn. (9) is discretized in time:

$$\frac{N_a(i+1) - N_a(i)}{\Delta t} = f[N_a(i)] \tag{10}$$

where:

$N_a(i)$—— Number of methane molecules in the adsorption zone of the i-th time step
Δt —— Time step

Substituting the initial conditions $N_a(0) = 245$ into Eq. (10), the number of molecules in the adsorption zone with time are obtained shown in Fig. 4. The results of molecular dynamics simulation are in good agreement with the results of the differential equation after 5 ps. The theoretical solution can basically reflect the situation of MDs, but there is one drawback that the theoretical solution slightly overestimated the decreasing rate of methane molecular number in the adsorption region in the dynamic process of the first 5 ps. Therefore, the theoretical model will be corrected below.

3.4. Diffusion delay correction

We previously assumed that the free zone of methane is evenly distributed to obtain Eq. (8), which is equivalent to ignore the free zone internal mass transfer resistance and consider that the mass transfer coefficient in the free zone is infinite. In fact, the mass transfer coefficient in the free zone is finite and there is a concentration gradient [11,12]. So its concentration near the adsorption area is greater than the average concentration, the pressure is also higher than the estimated value. Therefore, the original theory underestimates the microscopic adsorption rate in the microscopic desorption process. In order to further improve the accuracy of the original theoretical model, we will add to the free area within the mass transfer resistance correction.

In order to quantify this deviation, we need to study the mass transfer within the free zone. In order to simplify the analysis, it is assumed that the mass transfer coefficient inside the free zone is uniform and constant throughout the process. The semi-free-area is selected as the research object, and the mathematical description of its mass transfer behavior is:

$$\begin{cases} \dfrac{\partial n(z,t)}{\partial t} = D\dfrac{\partial^2 n(z,t)}{\partial z^2}, 0 < z < l, t > 0 \\ \dfrac{\partial n(0,t)}{\partial z} = -\dfrac{q(t)}{D}, \dfrac{\partial n(l,t)}{\partial z} = 0, t \geq 0 \\ n(z,0) = 0, 0 \leq z \leq l \end{cases} \tag{11}$$

where:

$n(z,t)$ —— Methane molecular density;
D —— Mass transfer coefficient;
l —— Half of the width of the free zone;
q —— Macroscopic desorption flow, equal to $J_d - J_a$

When q is a constant, the solution of Eq. (11) is:

$$n(0,t) = \sum_{n=1}^{\infty} -\frac{2ql}{D}\frac{1}{n^2}\exp\left(\frac{-Dn^2\pi^2 t}{l^2}\right) + \frac{ql}{2D} + \frac{q}{l}t = g(q,t) \tag{12}$$

when q is the amount $q(t)$ with time, according the superposition principle to obtain:

$$n(0,t) = \int_0^t g[dq(\tau), (t-\tau)] \tag{13}$$

Substituting Eq. (12) into Eqn. (13):

$$n(0,t) = \int_0^t -\frac{2l}{D}\frac{dq(\tau)}{d\tau}\sum_{n=1}^{\infty}\frac{1}{n^2}\exp\left[\frac{-Dn^2\pi^2(t-\tau)}{l^2}\right]d\tau + \frac{l}{2D}q(t)$$
$$+ \frac{1}{l}\int_0^t q(\tau)d\tau \tag{14}$$

The first term in the above formula indicates the effect of the previous concentration field on the current concentration field, and the impact is weakened over time. When the time interval exceeds a certain value, the effect can be ignored. The second term indicates that the concentration field is stable under the influence of the current macroscopic desorption flow when it is not affected by the previous concentration field. The third term represents the total amount of free methane. Eq. (14) is discretized in time step of 1 fs. The first term is omitted when $t - \tau > 5$fs, the items of n > 1 in the first infinite series is neglected when 5fs $\leq t - \tau \leq 5$fs and the items of n > 2 in the first infinite series is neglected when $t - \tau = 1$fs. So we have:

$$n(i) = \frac{N_f(i-1)}{2Sl} + \frac{l}{2D}q(i-1) - \sum_{n=1}^{5}\frac{2l}{D}[q(i-n) - q(i-n-1)]$$
$$\exp\left(-\frac{D\pi^2}{l^2}\right) - \frac{l}{4D}[q(i-1) - q(i-1)]\exp\left(-\frac{8D\pi^2}{l^2}\right) \tag{15}$$

when i < 5, some items do not exist, then these items should be ignored. The diffusion coefficient D is obtained by the average

pressure of the macroscopic desorption process, and the diffusion coefficient is 3.45×10^{-7} m^2/s in this paper.

The new pressure $P(i)$ taking into account the diffusion delay factor can be obtained by replacing n_f in Eq. (8) by $n(i)$ obtained by Eq. (15) multiplied by $2Sl$. Each time the old pressure is replaced by the new pressure, and complete the calculation similar to the previous calculation method. The theoretical predictions with diffusion delay correction are shown in Fig. 4. Compared with the old theoretical model, the theoretical model taking into account the diffusion factor is in good agreement with the results of molecular dynamics simulation. Compared to molecular dynamics simulation, the use of differential equations to describe the macroscopic desorption process can greatly reduce the amount of calculation, with a strong operability.

4. The effect of pressure, temperature and wall material on macroscopic desorption

In the previous section we derive the differential equation Eq. (5) describing the macroscopic desorption process and a time constant $T_0 = c_{sat}/(k_a P + k_d)$ can be obtained from a particular solution of the equation. So, the effect of temperature, pressure and wall material on macroscopic desorption are studied by the time constant. In order to obtain the methane saturation concentration of the solid-walled surface c_{sat}, the microscopic adsorption rate constant k_a and the macroscopic desorption rate constant k_d with different temperature and wall materials conditions, we carried out molecular dynamics simulation of four situations of 300 K graphite wall, 400 K Graphite wall , 353.5 K Quartz Wall and 353.5 K Kaolinite Wall. Quartz is the main component of the inorganic matrix containing gas shale, and kaolin is also an important place for clay minerals and shale gas adsorption. We use the CLATFF force field for quartz and kaolin. The results of the simulation are shown in Table 2 along with the results of the 353.5 K graphite wall.

From Table 2, it can be seen that the effect of temperature increase on c_{sat} is not significant, but k_a is significantly decreased and k_d is significantly increased with temperature increase. Under the same temperature condition, c_{sat}: quartz group $\approx$ kaolinite group > graphite group, k_a: quartz group > graphite group > kaolinite group, k_d: quartz group > kaolinite group > graphite group.

The expression of the time constant T_0 shows the pressure term. From Table 2, we can also know that how the other parameters are affected by the temperature and the wall material. Figs. 5 and 6 show the change of the time constant with pressure at different temperatures and the change of the time constant with pressure under different wall materials.

In general, the time constant decreases as the pressure increases, indicating that the higher the pressure, the higher the macroscopic desorption is to proceed. From the temperature point of view, the higher the temperature, the pressure change on the time constant the smaller the impact. The relative size relationship of time constants at different temperatures can vary with pressure. As shown in Fig. 5, when the pressure is less than 2 MPa, the time constant is 300 K > 353.5 K > 400 K; when the pressure is greater than 2 MPa, the time constant is 300 K < 353.5 K < 400 K. It shows that at lower pressure, the higher the temperature, the faster the

Table 2
Simulation results of c_{sat}, k_a and k_d under different conditions.

Temperature/Materials of Wall	c_{sat}/mol·m^{-2}	k_a/mol·m^{-2}·s^{-1}	k_d/mol·m^{-2}·s^{-1}
300 K/Graphite	1.67×10^{-5}	6.85×10^{5}	4.32×10^{6}
353.5/Graphite	1.69×10^{-5}	4.25×10^{5}	4.96×10^{6}
400 K/Graphite	1.77×10^{-5}	2.90×10^{5}	5.71×10^{6}
353.5/Quartz	2.05×10^{-5}	8.85×10^{5}	3.00×10^{7}
353.5/Kaolinite	2.04×10^{-5}	2.33×10^{5}	6.67×10^{6}
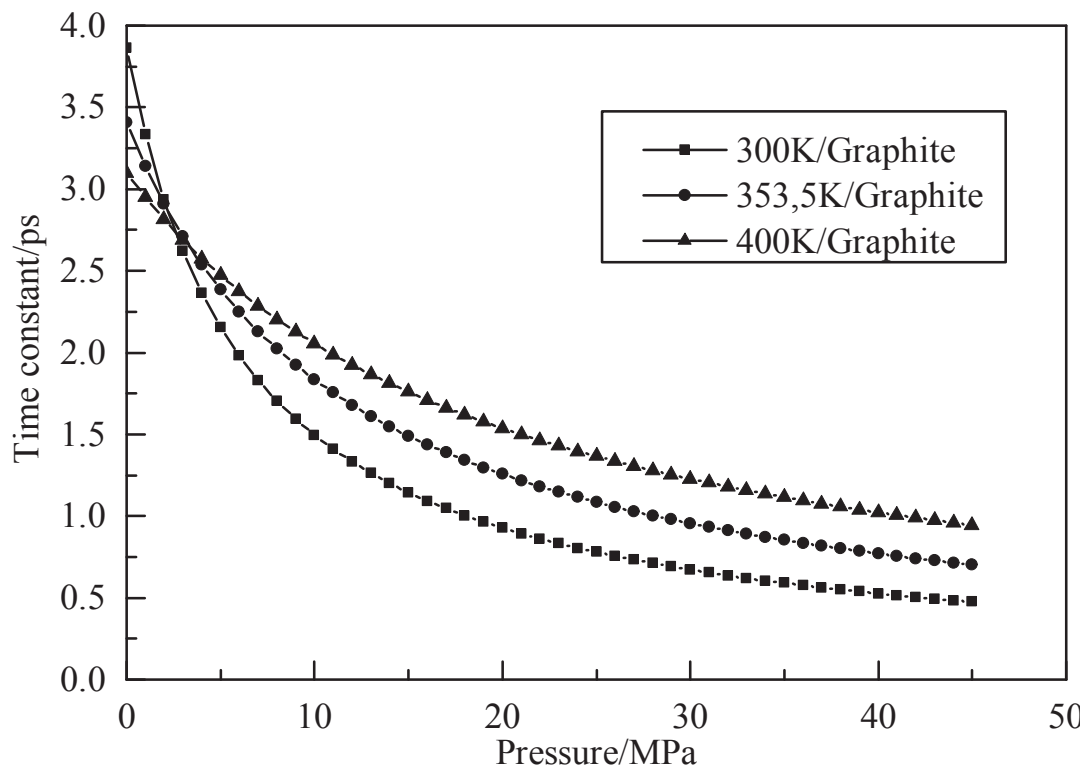
Fig. 5. The change of time constant with pressure at different temperature.
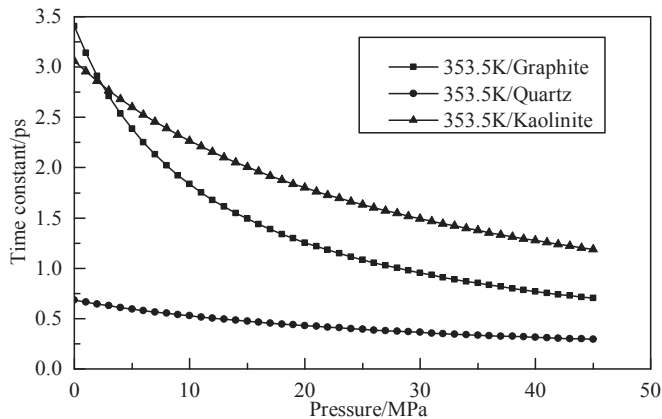
Fig. 6. The change of time constant with pressure under different wall materials.

macro-desorption proceeds; at higher pressure, the higher the temperature, the slower the macro-desorption proceeds. The difference in wall material will also affect the relative speed of macroscopic desorption. It can be seen from Fig. 6 that when the pressure is less than 2~3 MPa, the time constant: quartz < kaolinite < graphite; when the pressure is greater than 2~3 MPa and less than 45 MPa, the time constant: quartz < graphite < kaolinite. The effect of different wall materials on macroscopic desorption is related to the interaction between the wall and methane, which remains to be further studied.

5. Conclusions

In this paper, we establish differential equations to describe the macroscopic desorption process. A theoretical model taking into account the diffusion factor is presented, which can make the solution of the differential equation more suitable with the actual situation. And we get conclusions as follows:

1) The relationship between the amount of adsorbed methane in the equilibrium state and the pressure is consistent with the Langmuir isothermal adsorption curve. The microscopic adsorption rate and microscopic desorption rate of methane are also consistent with the Langmuir model.
2) Using the Langmuir model, the differential equations describing macroscopic desorption in slits are derived theoretically. The non-equilibrium desorption process was simulated by molecular dynamics, and a modified method for solving differential equations with free mass transfer is presented. After adding this correction, the solution of the differential equation is closer to the result of molecular dynamics simulation.
3) The effect of pressure, temperature and wall material on macroscopic desorption velocity was discussed by analyzing the time constant of macroscopic desorption process. Increased pressure will increase the speed of macroscopic desorption. The relationship between temperature and wall material is more complex, which is related to the difference of microscopic adsorption, desorption constant and saturated surface concentration of methane under different temperature and material conditions. At low pressure, the higher the temperature, the faster the desorption; at the high pressure, the higher the temperature, the lower the desorption. When pressure is low, the desorption speed at different wall material is quartz > kaolinite > graphite; when pressure is high, the desorption speed is quartz > graphite > kaolinite.

References

[1] Zeng M, Duan HM, Bai Y, Meng W. Forecasting the output of shale gas in China using an unbiased grey model and weakening buffer operator. Energy 2018;151:238—49.
[2] Seiichi K, Tatsuo N, Ikuo A. Adsorption science. second ed. Chemical Industry Press; 2005.
[3] Ji LM, Qiu JL, Xia YQ, Zhang TD. Electron microscopic scanning microporosity and methane adsorption of common clay minerals. J Pet Sci 2012;33(2):249—56.
[4] Simon JM, Haas OE, Kjelstrup S. Adsorption and desorption of H2 on graphite by molecular dynamics simulations. J Phys Chem C 2010;114(22):10212—20.
[5] Curtis JB. Fractured shale-gas system. AAPG Bull 2002;86(11):1921—38.
[6] Yu RZ, Bian YN, Zhang XW, Yan J, Zhao SY, Lin J. Summary of shale reservoir flow mechanism. Sci Technol Her 2012;30(24):75—9.
[7] Yao J, Sun H, Huang ZQ, Zhang L, Zeng DQ, Duo HG. Key mechanics problems in the development of shale gas reservoirs. Chin Sci Phys Mech Astron 2013;43(12):1527—47.
[8] Zhang JC, Jin ZJ, Yuan MS. Shale gas accumulation mechanism and distribution. Nat Gas Ind 2004;24(7):15—9.
[9] Ambrose RJ, Hartman RC, Campos MD, Akkutlu IY, Sondergeld CH. Shale gas-in-place calculations part I: New pore-scale considerations for shale gas in place calculations. SPE J 2012;17(1):219—29.
[10] Wang R, Zhang NS, Liu XJ, Wu XM, Yan J. Research progress of adsorption and desorption mechanism of shale gas. Sci Technol Eng 2013;13(19):5561—7.
[11] Shabro V, Torres-Verdin C, Javadpour F. Numerical simulation of shale-gas production: from pore-scale modeling of slip-flow, Knudsen diffusion, and Langmuir desorption to reservoir modeling of compressible fluid. In: Society of petroleum engineers - SPE Americas unconventional gas conference 2011. UGC; 2011. p. 706—16.
[12] Umeda K, Li R, Sawa Y, Yamabe H, Liang Y, Honda H, Murata S, Matsuoka T, Akai Takashi, Takagi S. Multiscale simulations of fluid flow in nanopores for shale gas. Int Pet Technol Conf 2014. https://doi.org/10.2523/IPTC-17949-MS.
[13] Liu B, Shi JQ, Shen Y, Zhang J. Molecular dynamics simulation of methane adsorption in graphite slits. Comput Phys 2013;30(05):692—9.
[14] Wang Q, Li SY, Li RR, Ma ML. Forecasting U.S. shale gas monthly production using a hybrid ARIMA and metabolic nonlinear grey model. Energy 2018;160:378—87.
[15] Ju Y, He J, Chang E, Zheng LG. Quantification of CH4 adsorption capacity in kerogen-rich reservoir shales: An experimental investigation and molecular dynamic simulation. Energy 2019;170:411—22.
[16] Khanal A, Khoshghadam M, Lee WJ, Nikolaou M. New forecasting method for liquid rich shale gas condensate reservoirs with data driven approach. J Nat Gas Sci Eng 2017;38:621—37.
[17] Yang XL, Li B, Peng CS, Yang Y. Application of a wide-field electromagnetic method to shale gas exploration in South China. Appl Geophys 2017;14(3):441—8.
[18] Chang Y, Huang RZ, Ries RJ, Masanet E. Life-cycle comparison of greenhouse gas emissions and water consumption for coal and shale gas fired power generation in China. Energy 2015;86:335—43.
[19] Kiv IR, Zare-Reisabadi M, Saemi M, Zamani Z. An intelligent approach to brittleness index estimation in gas shale reservoirs: A case study from a western Iranian basin. J Nat Gas Sci Eng 2017;44:177—90.
[20] McGlade C, Speirs J, Sorrell S. Methods of estimating shale gas resources e Comparison, evaluation and implications. Energy 2013;59:116—25.
[21] Medlock III KB. Shale gas, emerging fundamentals, and geopolitics. In: SPEGCS general meeting. Houston, TX: James A Baker III Institute for Public Policy Rice University; 2012.
[22] Umeozor EC, Jordaan SM, Gates ID. On methane emissions from shale gas development. Energy 2018;152:594—600.
[23] Brandt AR, et al. Methane leaks from North American natural gas systems. Science 2014;343(6172):733—5.
[24] Littlefield JA, et al. Using common boundaries to assess methane emissions: A life cycle evaluation of natural gas and coal power systems. J Ind Ecol 2016;20(6):1360—9.
[25] Lamb BK, et al. Direct and indirect measurements and modeling of methane emissions in Indianapolis, Indiana. Environ Sci Technol 2016;50(16):8910—7.
[26] Tan SH, Barton PI. Optimal shale oil and gas investments in United States. Energy 2017;141:398—422.
[27] Knudsen BR, Foss B. Shut-in based production optimization of shale-gas systems. Comput Chem Eng 2013;58:54e67.
[28] Knudsen BR, Grossmann IE, Foss B, Conn AR. Lagrangian relaxation based decomposition for well scheduling in shale-gas systems. Comput Chem Eng 2014;63:234—49.
[29] Knudsen BR, Whitson CH, Foss B. Shale-gas scheduling for natural-gas supply in electric power production. Energy 2014;78:165—82.

[30] Bistline JE. Natural gas, uncertainty, and climate policy in the US electric power sector. Energy Policy 2014;74:433—42.

[31] Cafaro DC, Grossmann IE. Strategic planning, design, and development of the shale gas supply chain network. AIChE J 2014;60(6):2122—42.

[32] Yang L, Grossmann IE, Manno J. Optimization models for shale gas water management. AIChE J 2014;60(10):3490—501.

[33] Tae HK, Cho JH, Lee KS. Evaluation of CO2 injection in shale gas reservoirs with multi-component transport and geomechanical effects. Appl Energy 2017;190:1195—206.

[34] He JL, Wang J, Yu Q, Liu W, Ge XY, Yang P, Wang ZJ, Lu JZ. Pore structure of shale and its effects on gas storage and transmission capacity in well HD-1 eastern Sichuan Basin, China. Fuel 2018;226:709—20.

[35] Hao F, Zou H, Lu Y. Mechanisms of shale gas storage: Implications for shale gas exploration in China. AAPG Bull 2013;97:1325—46.

[36] Dai J, Zou C, Dong D, Ni Y, Wu W, Gong D, et al. Geochemical characteristics of marine and terrestrial shale gas in China. Mar Petrol Geol 2016;76:444—63.

[37] Ye ZH, Chen D, Pan XJ, Zhang GQ, Xia Y, Ding X. An improved Langmuir model for evaluating methane adsorption capacity in shale under various pressures and temperatures. J Nat Gas Sci Eng 2016;31:658—80.

[38] Tang X, Ripepi N, Stadie NP, Yu LJ, Hall MR. A dual-site Langmuir equation for accurate estimation of high pressure deep shale gas resources. Fuel 2016;185:10—7.

[39] Jin Q, Huang LM, Li AM, Shan AD. Quantification of the limitation of Langmuir model used in adsorption research on sediments energy heterogeneity. Chemosphere 2017;185:518—28.

[40] Ofomaja AEO, Unuabonah EI. Kinetics and time-dependent Langmuir modeling of 4-nitrophenol adsorption onto Mansonia sawdust. J. Taiwan Inst Chem Eng 2013;44(4):566—76.

[41] Singh H, Javadpour F. Langmuir slip-Langmuir sorption permeability model of shale. Fuel 2016;164:28—37.

[42] Yang Y, Liu SM, Zhao W, Wang L. Intrinsic relationship between Langmuir sorption volume and pressure for coal: Experimental and thermodynamic modeling study. Fuel 2019;241:105—17.